



## Parameter estimation for peaky altimetric waveforms

Abderrahim Halimi, Corinne Mailhes, Jean-Yves Tourneret, Pierre Thibault,  
François Boy

### ► To cite this version:

Abderrahim Halimi, Corinne Mailhes, Jean-Yves Tourneret, Pierre Thibault, François Boy. Parameter estimation for peaky altimetric waveforms. IEEE Transactions on Geoscience and Remote Sensing, Institute of Electrical and Electronics Engineers, 2013, vol. 51, pp.1568-1577. <10.1109/TGRS.2012.2205697>. <hal-00800065>

**HAL Id: hal-00800065**

**<https://hal.archives-ouvertes.fr/hal-00800065>**

Submitted on 13 Mar 2013

**HAL** is a multi-disciplinary open access archive for the deposit and dissemination of scientific research documents, whether they are published or not. The documents may come from teaching and research institutions in France or abroad, or from public or private research centers.

L'archive ouverte pluridisciplinaire **HAL**, est destinée au dépôt et à la diffusion de documents scientifiques de niveau recherche, publiés ou non, émanant des établissements d'enseignement et de recherche français ou étrangers, des laboratoires publics ou privés.



**Open Archive TOULOUSE Archive Ouverte (OATAO)**  
OATAO is an open access repository that collects the work of Toulouse researchers and makes it freely available over the web where possible.

This is an author-deposited version published in : <http://oatao.univ-toulouse.fr/>  
Eprints ID : 8501

To link to this article : DOI:10.1109/TGRS.2012.2205697  
URL : <http://dx.doi.org/10.1109/TGRS.2012.2205697>

To cite this version :

Halimi, Abderrahim and Mailhes, Corinne and Tourneret, Jean-Yves and Thibault, Pierre and Boy, François *Parameter estimation for peaky altimetric waveforms*. (2013) IEEE Transactions on Geoscience and Remote Sensing, vol. 51 (n° 3). pp. 1568-1577. ISSN 0196-2892

Any correspondence concerning this service should be sent to the repository administrator: [staff-oatao@listes.diff.inp-toulouse.fr](mailto:staff-oatao@listes.diff.inp-toulouse.fr)

# Parameter Estimation for Peaky Altimetric Waveforms

Abderrahim Halimi, *Student Member, IEEE*, Corinne Mailhes, *Member, IEEE*, Jean-Yves Tourneret, *Senior Member, IEEE*, Pierre Thibaut, and Francois Boy

**Abstract**—Much attention has been recently devoted to the analysis of coastal altimetric waveforms. When approaching the coast, altimetric waveforms are sometimes corrupted by peaks caused by high reflective areas inside the illuminated land surfaces or by the modification of the sea state close to the shoreline. This paper introduces a new parametric model for these peaky altimetric waveforms. This model assumes that the received altimetric waveform is the sum of a Brown echo and an asymmetric Gaussian peak. The asymmetric Gaussian peak is parameterized by a location, an amplitude, a width, and an asymmetry coefficient. A maximum-likelihood estimator is studied to estimate the Brown plus peak model parameters. The Cramér–Rao lower bounds of the model parameters are then derived providing minimum variances for any unbiased estimator, i.e., a reference in terms of estimation error. The performance of the proposed model and the resulting estimation strategy are evaluated via many simulations conducted on synthetic and real data. Results obtained in this paper show that the proposed model can be used to retrack efficiently standard oceanic Brown echoes as well as coastal echoes corrupted by symmetric or asymmetric Gaussian peaks. Thus, the Brown with Gaussian peak model is useful for analyzing altimetric measurements closer to the coast.

**Index Terms**—Brown model, coastal altimetry, Cramér–Rao bounds (CRBs), maximum likelihood (ML), peaks.

## I. INTRODUCTION

OVER an ocean surface, the altimetric echo has a well-defined shape, with a steeply rising leading edge followed by a gradual decline in power over the rest of the waveform called trailing edge [1], [2]. This well-defined shape is accurately modeled by the Brown model [1], [3], [4]. Many different algorithms have been proposed in the literature to estimate the parameters of the Brown model. These algorithms are, for instance, based on the maximum likelihood (ML) principle [5], [6], the least squares method [7], [8], or, more recently, on Bayesian inference [9]. However, the altimetric waveform can be corrupted by land returns, by rain [10], [11], or by the summation of backscattered signals coming from separate

A. Halimi, C. Mailhes, and J.-Y. Tourneret are with the University of Toulouse, Institut de Recherche en Informatique de Toulouse, 31071 Toulouse Cedex 7, France (e-mail: Abderrahim.Halimi@enseiht.fr; Corinne.Mailhes@enseiht.fr; Jean-Yves.Tourneret@enseiht.fr).

P. Thibaut is with Collecte Localisation Satellites, 31520 Ramonville Saint-Agne, Toulouse, France (e-mail: pthibaut@cls.fr).

F. Boy is with Centre National d'Études Spatiales, 31401 Toulouse Cedex 9, France (e-mail: Francois.Boy@cnes.fr).

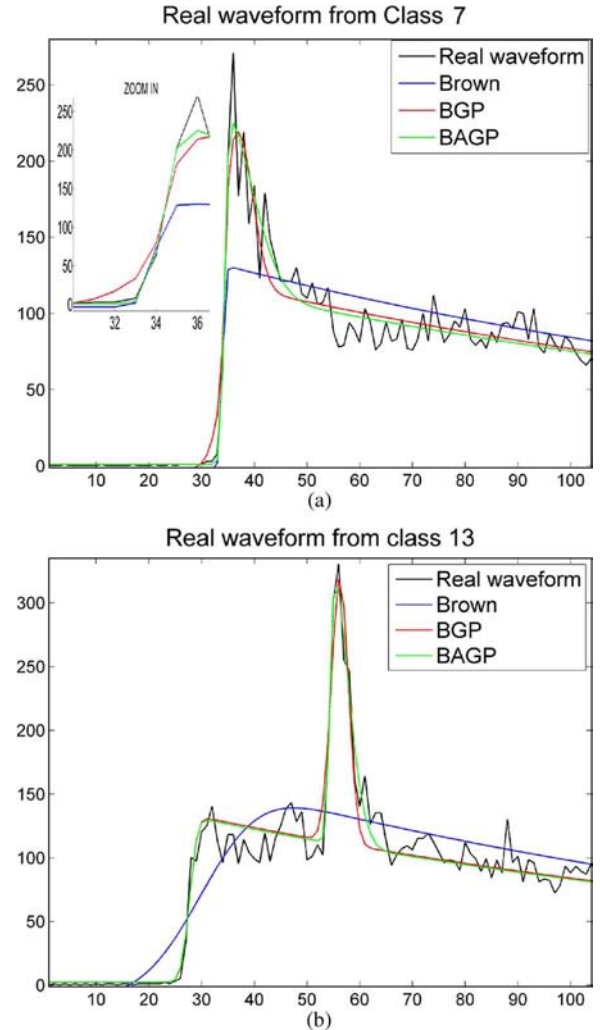


Fig. 1. Examples of real JASON-2 waveforms and their estimations. (a) Real waveform from Class 7 and its estimates. (b) Real waveform from Class 13 and its estimates.

reflective ocean surfaces which make these algorithms ineffective. This inefficiency is illustrated in Fig. 1 which shows two representative coastal Jason-2 waveforms (black curves) and their estimates resulting from the ML estimator (MLE) applied to the Brown model (blue curves). Due to the presence of a peak at the end of the leading edge [see Fig. 1(a)] or in the middle of the trailing edge [see Fig. 1(b)], the Brown model is clearly unable to capture the variations of the altimetric echo. A great effort is now devoted to process coastal waveforms in order to move the altimetric measurements closer to the

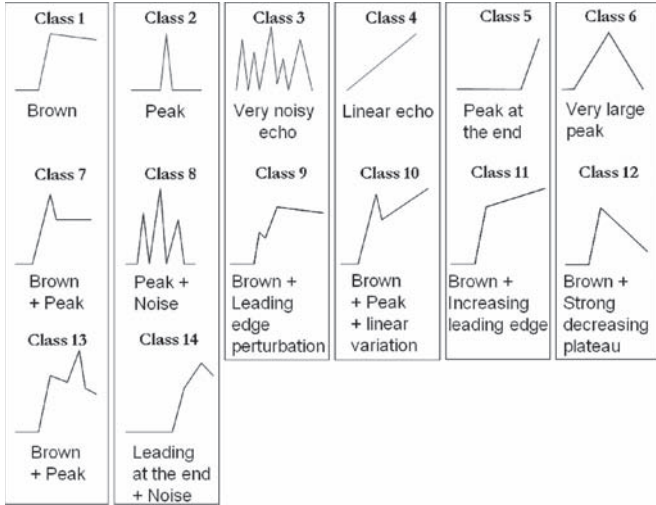


Fig. 2. Different shapes of altimetric signals resulting from CNES/PISTACH project.

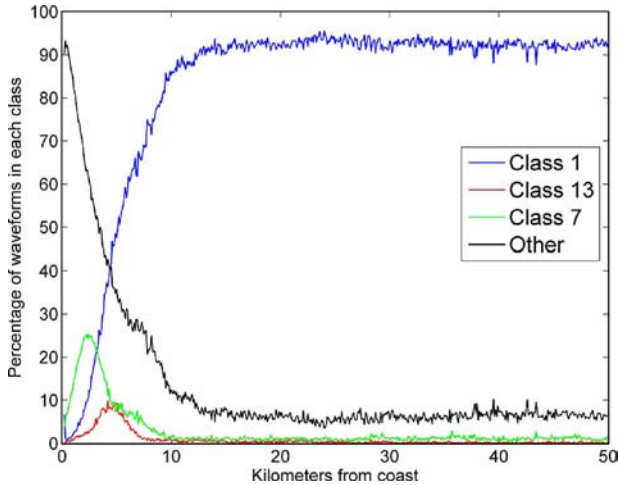


Fig. 3. Percentages of observed altimetric waveforms in Classes 1, 7, 13, and others versus distance to the coast.

coast [12], [13]. The analysis of coastal waveforms has been recently considered intensively in two projects, the PISTACH [14]<sup>1</sup> and the COASTALT [15].<sup>2</sup> In the frame of the PISTACH project aiming at improving coastal altimeter products, waveforms are classified according to geometrical shapes shown in Fig. 2 [16]. The goal of this classification is to isolate echoes having similar geometrical characteristics in order to estimate the corresponding altimeter parameters thanks to dedicated so-called retracking algorithms. As shown in Fig. 2, several signal classes investigated in the PISTACH project are characterized by signals corrupted by peaks. These signals are frequently observed in the coastal areas. More precisely, in open ocean, about 95% of the waveforms are in good agreement with the Brown model. However, when approaching the coasts (or over polar surfaces), this percentage rapidly decreases. As shown in Fig. 3, roughly 25% to 30% of the waveforms are not Brownian at a distance of 8 km off the shorelines.

<sup>1</sup>The PISTACH project has been funded by Centre National d'Etudes Spatiales (CNES).

<sup>2</sup>The COASTALT project has been funded by the European Space Agency.

This paper introduces a parametric model for peaky altimetric signals (similar to those classified in Classes 7 and 13 of Fig. 2) referred to as the Brown with asymmetric Gaussian peak (BAGP) model. The BAGP model is appropriate for signals defined as the sum of a Brown echo and a Gaussian peak. The idea of using Gaussian shapes to model peaks in altimetric waveforms has appeared in [17] and [18]. However, the model studied in this paper is more general since it allows peak asymmetry to be considered. Peak asymmetry is clearly important for signals of Class 7 characterized by an asymmetric peak located at the end of the leading edge [see Fig. 1(a) for an example]. An interesting property of the proposed BAGP model is that it reduces to the classical Brown model when the amplitude of the peak is zero. Thus, one can expect similar performance with this model and the classical Brown model for oceanic waveforms as well as improved signal reconstructions for waveforms corrupted by peaks. Moreover, it is interesting to note that the BAGP model can handle symmetric peaks affecting the altimetric waveform when the asymmetry coefficient is set to zero. Thus, the BAGP model should also be able to model accurately altimetric waveforms from Class 13 [see Fig. 1(b) for an example]. To summarize, the proposed BAGP model is appropriate for usual oceanic waveforms as well as coastal waveforms corrupted by either a symmetric or an asymmetric peak.

In order to estimate the unknown BAGP model parameters, we propose to use the ML method that has shown interesting results for the classical Brown model [5], [6]. Closed-form expressions of the MLE for the BAGP model parameters are difficult to obtain. As a consequence, numerical algorithms are considered for computing this estimator. The first algorithm is based on a Newton–Raphson (NR) strategy, similar to the one investigated in [5] and [19]. A second algorithm based on a geometrical technique known as the Nelder–Mead (NM) method [20] is also studied. The Cramér–Rao bounds (CRBs) associated with the BAGP model parameters are finally determined. These bounds are interesting since they provide the minimum variance of any unbiased estimator. Another interesting property of these bounds is that the variance of any MLE can be approximated for large sample size by its corresponding CRB under weak conditions. These conditions are, for instance, specified in [21, Chap. 18] (we mainly have to check that the range of the likelihood does not depend on the unknown parameters and that the likelihood is a twice differentiable function of its unknown parameters throughout its range).

This paper is structured as follows. Section II presents the BAGP model considered in this study. Relationships between the BAGP, the Brown model, and the Brown with Gaussian peak model introduced in [18] are also studied. The likelihood associated with the BAGP model is derived in Section III. Section IV introduces the different algorithms used to maximize the likelihood of the BAGP model. Section V derives the CRBs of the BAGP model parameters. Simulation results obtained with synthetic data are analyzed in Section VI, whereas an analysis of real Jason-2 waveforms is presented in Section VII. Conclusions and future works are finally reported in Section VIII.

## II. WAVEFORM MODEL

A simplification of the Brown model assumes that the altimetric waveform, associated with oceanic surfaces, is characterized by three parameters, the amplitude  $P_u$ , the epoch  $\tau$ , and the significant wave height SWH. The resulting mathematical model for the altimetric signal is

$$s_k = \frac{P_u}{2} \left[ 1 + \operatorname{erf} \left( \frac{kT_s - \tau - \alpha \sigma_c^2}{\sqrt{2} \sigma_c} \right) \right] e^{-\alpha \left( kT_s - \tau - \frac{\alpha \sigma_c^2}{2} \right)} + N_t \quad (1)$$

with

$$\sigma_c^2 = \left( \frac{\text{SWH}}{2c} \right)^2 + \sigma_p^2 \quad (2)$$

where  $s_k = s(kT_s)$  is the  $k$ th data sample of the received altimetric signal,  $T_s$  is the sampling period,  $\operatorname{erf}(t) = (2/\sqrt{\pi}) \int_0^t e^{-z^2} dz$  stands for the Gaussian error function,  $c$  denotes the speed of light,  $\alpha$  and  $\sigma_p^2$  are two known parameters (depending on the satellite and on the point target response of the altimeter), and  $N_t$  is the instrument thermal noise. The additive noise parameter  $N_t$  is generally estimated using the first data samples and subtracted from the observed samples  $s_k$ , resulting in  $N_t = 0$  in model (1). The model (1) has received considerable attention in the literature and has been shown to be very accurate for oceanic waveforms. However, it is inappropriate for modeling altimetric waveforms backscattered from nonoceanic surfaces such as ice and land or from coastal areas [16]–[18]. Indeed, over such surfaces, altimetric echoes can show some peaks in their trailing edge due to backscattering returns from nonwater areas. Therefore, this paper studies a new model (referred to as BAGP for Brown Asymmetric Gaussian Peak) defined as the superposition of a Brown echo  $s_k$  and an asymmetric Gaussian peak  $p_k$  such that the observed signal is

$$\tilde{s}_k = s_k + p_k \quad (3)$$

with

$$p_k = A \exp \left[ \frac{-1}{2\sigma^2} (kT_s - T)^2 \right] \left\{ 1 + \operatorname{erf} \left[ \gamma \frac{(kT_s - T)}{\sqrt{2}} \right] \right\} \quad (4)$$

where  $A$ ,  $T$ ,  $\sigma$ , and  $\gamma$  are the amplitude, location, width, and asymmetry coefficient of the peak. It is interesting to note that the Gaussian peak defined in (4) reduces to a symmetric Gaussian peak when  $\gamma = 0$  (thus, the parameter  $\gamma$  will be referred to as an asymmetry coefficient in this paper). The resulting model parameterized by  $A$ ,  $T$ , and  $\sigma$  is referred to as the BGP model (for Brown Gaussian Peak model). Note also that the BAGP and BGP models reduce to the Brown model for  $A = 0$ . Fig. 4 shows the effect of the asymmetry coefficient  $\gamma$  on the normalized peak  $p_k$  defined in (4). A positive value of  $\gamma$  squeezes the left side of the peak while a negative value squeezes its right side. Note that, for real JASON-2 waveforms, the estimated values of  $\gamma$  are mainly positive and located near 0 (see [22] for more details).

The next section introduces an ML estimation method to estimate the unknown parameter vector associated with the BAGP model defined by (3) and (4). These unknown parameters are shown in Table I.

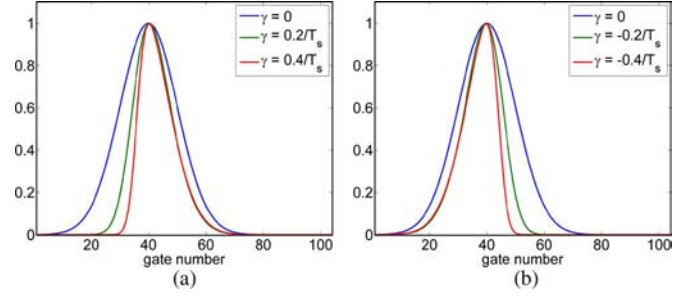


Fig. 4. Effect of the asymmetry coefficient on the peak.

TABLE I  
DESCRIPTION OF THE MODEL PARAMETERS

Name	Description
$P_u$	Amplitude of Brown's waveform
$\tau$	Epoch
SWH	Significant wave height
$A$	Amplitude of the peak
$T$	Location of the peak
$\sigma$	Standard deviation of the Gaussian peak
$\gamma$	Asymmetry coefficient of the peak

## III. MAXIMUM LIKELIHOOD ESTIMATOR

Altimeter data are corrupted by multiplicative speckle noise. In order to reduce the influence of this noise affecting each individual echo, a sequence of  $L$  consecutive echoes are averaged on board the satellite. Assuming pulse-to-pulse statistical independence (which is a valid assumption for Jason [23]), the resulting speckle noise sequence is independent and identically distributed according to a gamma distribution whose shape and scale parameters equal the number of looks  $L$ , i.e., the number of incoherent summations of consecutive echoes. When using the BAGP model defined in (3), an observed altimetric waveform can be expressed as

$$y_k = \tilde{s}_k n_k, \quad k = 1, \dots, K \quad (5)$$

where  $K$  is the number of samples. Using (5) and the properties of the noise sequence  $\mathbf{n} = (n_1, \dots, n_K)^T$ , the likelihood function of the observed samples  $f(\mathbf{y}|\boldsymbol{\theta})$  can be expressed as follows:

$$f(\mathbf{y}|\boldsymbol{\theta}) = \left[ \frac{L^L}{\Gamma(L)} \right]^K \exp \left( -L \sum_{k=1}^K \frac{y_k}{\tilde{s}_k} \right) \left( \prod_{k=1}^K y_k \right)^{L-1} \times \left( \prod_{k=1}^K \tilde{s}_k \right)^{-L} \left( \prod_{k=1}^K \mathcal{I}_{\mathbb{R}^+}(y_k) \right) \quad (6)$$

where  $\mathbf{y} = (y_1, \dots, y_K)^T$ ,  $\boldsymbol{\theta}_B = (P_u, \tau, \text{SWH})^T$ , and  $\boldsymbol{\theta}_p = (A, T, \sigma, \gamma)^T$  contain the unknown Brown and peak parameters,  $\boldsymbol{\theta} = (\boldsymbol{\theta}_B^T, \boldsymbol{\theta}_p^T)^T$ , and  $\mathcal{I}_{\mathbb{R}^+}(y_k)$  is the indicator function ( $\mathcal{I}_{\mathbb{R}^+}(y_k) = 1$  if  $y_k \in \mathbb{R}^+$ , and  $\mathcal{I}_{\mathbb{R}^+}(y_k) = 0$  otherwise). The MLE of  $\boldsymbol{\theta}$  (denoted as  $\hat{\boldsymbol{\theta}}_{\text{MLE}}$ ) is obtained by maximizing the likelihood function  $f(\mathbf{y}|\boldsymbol{\theta})$  with respect to  $\boldsymbol{\theta}$  or, equivalently,

by minimizing the negative log-likelihood that reduces to the following cost function

$$C = L \sum_{k=1}^K \frac{y_k}{\tilde{s}_k} + L \sum_{k=1}^K \ln(\tilde{s}_k) \quad (7)$$

after removing unnecessary constants. The MLE of  $\boldsymbol{\theta}$  cannot be computed in closed form even in the case of a classical Brown model where there is no peak in the altimetric signal model. Consequently, numerical optimization techniques have to be used to implement the MLE. Two approaches have been investigated in this paper based on the NR [24] and NM [20] methods. These methods are presented in the next section.

#### IV. ESTIMATION ALGORITHMS

##### A. NR Method

The estimation of the BAGP parameters can be achieved by generalizing the NR algorithm commonly used to estimate the Brown model parameters. This section first summarizes the main steps of the NR algorithm when applied to the Brown model. A generalization to the BAGP model is then presented.

1) *NR Method for Brown Model*: The NR method is an iterative algorithm that updates the parameters to be estimated according to the following recursion:

$$\boldsymbol{\theta}_B(n+1) = \boldsymbol{\theta}_B(n) - \psi(n) \mathbf{H}_B^{-1}(n) \nabla \mathcal{C}_B(n) \quad (8)$$

where  $\boldsymbol{\theta}_B = (P_u, \tau, \text{SWH})^T = (\theta_{B,1}, \theta_{B,2}, \theta_{B,3})^T$ ,  $\psi(n)$  is a step size belonging to the interval  $[0, 1]$  (ensuring the convergence of the algorithm),  $\nabla$  is the gradient operator, and  $\mathbf{H}_B$  is a symmetric and invertible matrix defined as the Hessian of the cost function  $\mathcal{C}_B$  which is obtained by setting  $\tilde{s}_k = s_k$  in (7). The gradient of the cost function  $\mathcal{C}_B$  [of size  $(3 \times 1)$ ] with respect to the Brown vector parameters  $\boldsymbol{\theta}_B$  is given by

$$\begin{aligned} \nabla \mathcal{C}_B &= \left( -\frac{\partial \ln [f_B(\mathbf{y}|\boldsymbol{\theta}_B)]}{\partial \theta_{B,i}} \right)_{i=1,\dots,3}^T \\ &= L \left( \sum_{k=1}^K \frac{s_k - y_k}{s_k^2} \frac{\partial s_k}{\partial \theta_{B,i}} \right)_{i=1,\dots,3}^T \end{aligned} \quad (9)$$

where  $f_B$  is the likelihood obtained by setting  $\tilde{s}_k = s_k$  and  $\boldsymbol{\theta} = \boldsymbol{\theta}_B$  in (6). More precisely, (9) can be expressed as

$$\nabla \mathcal{C}_B = L \mathbf{B}_B \mathbf{d}_B \quad (10)$$

where  $\mathbf{d}_B = (d_k)_{k=1,\dots,K}$  is a  $(K \times 1)$  vector with  $d_k = (s_k - y_k)/s_k$  and  $\mathbf{B}_B$  is a matrix whose components are  $B_{i,k} = (1/s_k)(\partial s_k / \partial \theta_{B,i})$ , for  $i = 1, \dots, 3$  and  $k = 1, \dots, K$ .

In order to reduce the computational complexity due to the calculation of the Hessian at each iteration, an approximation

of this matrix is generally used. This approximation replaces the matrix  $\mathbf{H}_B$  by its expectation

$$\mathbf{F}_B = E[\mathbf{H}_B] = -E \begin{bmatrix} \frac{\partial^2 \ln f_B}{\partial \theta_{B,1}^2} & \frac{\partial^2 \ln f_B}{\partial \theta_{B,1} \theta_{B,2}} & \frac{\partial^2 \ln f_B}{\partial \theta_{B,1} \theta_{B,3}} \\ \frac{\partial^2 \ln f_B}{\partial \theta_{B,2} \theta_{B,1}} & \frac{\partial^2 \ln f_B}{\partial \theta_{B,2}^2} & \frac{\partial^2 \ln f_B}{\partial \theta_{B,2} \theta_{B,3}} \\ \frac{\partial^2 \ln f_B}{\partial \theta_{B,3} \theta_{B,1}} & \frac{\partial^2 \ln f_B}{\partial \theta_{B,3} \theta_{B,2}} & \frac{\partial^2 \ln f_B}{\partial \theta_{B,3}^2} \end{bmatrix} \quad (11)$$

where  $E$  stands for the mathematical expectation. Note that the matrix  $\mathbf{F}_B$  is the Fisher information matrix (FIM) that is commonly used to compute the CRBs [25]. The iterative formula obtained after replacing  $\mathbf{H}_B$  by  $\mathbf{F}_B$  in (8) is

$$\boldsymbol{\theta}_B(n+1) = \boldsymbol{\theta}_B(n) - \psi(n) \mathbf{F}_B^{-1}(n) \nabla \mathcal{C}_B(n). \quad (12)$$

This parameter recursion has shown interesting properties for adaptive filtering and is sometimes referred to as Fisher scoring [26]. Determining the matrix  $\mathbf{F}_B$  requires to compute the expectations of the second-order derivatives of  $f_B$ . It is straightforward to show that

$$E \left[ -\frac{\partial^2 \ln f_B}{\partial \theta_{B,i} \partial \theta_{B,j}} \right] = L \sum_{k=1}^K \frac{1}{s_k^2} \frac{\partial s_k}{\partial \theta_{B,i}} \frac{\partial s_k}{\partial \theta_{B,j}}. \quad (13)$$

As a consequence, the matrix  $\mathbf{F}_B$  can be written as  $\mathbf{F}_B = L \mathbf{B}_B \mathbf{B}_B^T$ , and the recursive formula (12) reduces to

$$\boldsymbol{\theta}_B(n+1) = \boldsymbol{\theta}_B(n) - \psi(n) (\mathbf{B}_B \mathbf{B}_B^T)^{-1} \mathbf{B}_B \mathbf{d}_B. \quad (14)$$

2) *NR Method for the BAGP*: In order to generalize the previous NR recursion to the BAGP model, we introduce a  $(3 \times K)$  matrix  $\tilde{\mathbf{B}}$  whose elements are  $\tilde{B}_{i,k} = (1/\tilde{s}_k)(\partial \tilde{s}_k / \partial \theta_{B,i})$  with  $i = 1, \dots, 3$  and  $k = 1, \dots, K$ , a  $(4 \times K)$  matrix  $\tilde{\mathbf{P}}$  whose elements are  $\tilde{P}_{i,k} = (1/\tilde{s}_k)(\partial p_k / \partial \theta_{p,i})$  with  $i = 1, \dots, 4$  and  $k = 1, \dots, K$ , and a  $(K \times 1)$  vector  $\tilde{\mathbf{d}}$  with components  $\tilde{d}_k = (\tilde{s}_k - y_k)/\tilde{s}_k$ . The unknown parameter vector for the BAGP is  $\boldsymbol{\theta} = (\boldsymbol{\theta}_B^T, \boldsymbol{\theta}_p^T)^T = (\theta_1, \theta_2, \dots, \theta_7)^T$ . We propose to estimate  $\boldsymbol{\theta}$  using the following recursive formula:

$$\boldsymbol{\theta}(n+1) = \boldsymbol{\theta}(n) - \psi(n) \mathbf{F}^{-1}(n) \nabla \mathcal{C}(n) \quad (15)$$

where  $\mathbf{F}(n)$  and  $\nabla \mathcal{C}(n)$  are the FIM and gradient of  $\mathcal{C}$  evaluated at  $\boldsymbol{\theta} = \boldsymbol{\theta}(n)$ . Straightforward computations lead to

$$\begin{aligned} \mathbf{F} &= -E \begin{bmatrix} \frac{\partial^2 \ln f}{\partial \theta_1^2} & \frac{\partial^2 \ln f}{\partial \theta_1 \theta_2} & \cdots & \frac{\partial^2 \ln f}{\partial \theta_1 \theta_7} \\ \frac{\partial^2 \ln f}{\partial \theta_2 \theta_1} & \frac{\partial^2 \ln f}{\partial \theta_2^2} & \cdots & \frac{\partial^2 \ln f}{\partial \theta_2 \theta_7} \\ \frac{\partial^2 \ln f}{\partial \theta_7 \theta_1} & \frac{\partial^2 \ln f}{\partial \theta_7 \theta_2} & \cdots & \frac{\partial^2 \ln f}{\partial \theta_7^2} \end{bmatrix} \\ &= L \begin{pmatrix} \tilde{\mathbf{B}} \tilde{\mathbf{B}}^T & \tilde{\mathbf{B}} \tilde{\mathbf{P}}^T \\ \tilde{\mathbf{P}} \tilde{\mathbf{B}}^T & \tilde{\mathbf{P}} \tilde{\mathbf{P}}^T \end{pmatrix} \end{aligned} \quad (16)$$

$$\nabla \mathcal{C} = L \begin{pmatrix} \tilde{\mathbf{B}} \\ \tilde{\mathbf{P}} \end{pmatrix} \tilde{\mathbf{d}}. \quad (17)$$

As a consequence, the NR recursion (15) can be written

$$\boldsymbol{\theta}(n+1) = \boldsymbol{\theta}(n) - \psi(n) \begin{pmatrix} \tilde{\mathbf{B}} \tilde{\mathbf{B}}^T & \tilde{\mathbf{B}} \tilde{\mathbf{P}}^T \\ \tilde{\mathbf{P}} \tilde{\mathbf{B}}^T & \tilde{\mathbf{P}} \tilde{\mathbf{P}}^T \end{pmatrix}^{-1} \begin{pmatrix} \tilde{\mathbf{B}} \\ \tilde{\mathbf{P}} \end{pmatrix} \tilde{\mathbf{d}}. \quad (18)$$

## B. NM Method

The NM method is a simplex method for nonlinear unconstrained optimization used for minimizing an objective function in a many-dimensional subspace [20], [27]. This direct search method does not use any information (explicit or implicit) about the derivatives of the cost function. By considering  $m$  as the length of the parameter vector to estimate ( $m = 3$  for the Brown model,  $m = 6$  for the BGP, and  $m = 7$  for the BAGP), the NM algorithm<sup>3</sup> works in an  $m$ -dimensional subspace that is characterized by  $m + 1$  distinct vectors that are its vertices and their associated function values. At each step of the search, a new point in or near the current simplex<sup>4</sup> is generated. The cost function is evaluated at the new generated point and compared with its values at the vertices of the simplex. When the cost function is smaller at the generated point, one of the vertices is replaced by this generated point, giving a new simplex. This step is repeated until the diameter of the simplex is less than a specified tolerance (see [20], [24], and [27] for more details).

## V. CRAMÉR-RAO BOUNDS

The CRBs provide the minimum variances for unbiased parameters. As a consequence, they can be considered as references in terms of estimation errors. Comparing the mean square errors (MSEs) of estimators to the corresponding CRBs helps us to understand the potential gain in performance that we might obtain with other estimation algorithms. The CRBs for the parameters of the Brown model were derived in [25]. This section generalizes the results of [25] to the BAGP model. The CRBs are obtained by inverting the FIM of  $\theta$ . Since the thermal noise parameter  $N_t$  has been estimated using the first samples of the altimetric signal, it also has to be included in the FIM, resulting in the  $(8 \times 8)$  matrix

$$\mathbf{F}_{\text{CRB}} = -E \begin{bmatrix} \frac{\partial^2 \ln f}{\partial \theta_1^2} & \frac{\partial^2 \ln f}{\partial \theta_1 \theta_2} & \cdots & \frac{\partial^2 \ln f}{\partial \theta_1 N_t} \\ \frac{\partial^2 \ln f}{\partial \theta_1 \theta_2} & \frac{\partial^2 \ln f}{\partial \theta_2^2} & \cdots & \frac{\partial^2 \ln f}{\partial \theta_2 N_t} \\ \frac{\partial^2 \ln f}{\partial \theta_1 N_t} & \frac{\partial^2 \ln f}{\partial \theta_2 N_t} & \cdots & \frac{\partial^2 \ln f}{\partial N_t^2} \end{bmatrix} \quad (19)$$

whose elements are given by

$$E \left[ -\frac{\partial^2 \ln f}{\partial \theta_i \partial \theta_j} \right] = L \sum_{k=1}^K \frac{1}{\tilde{s}_k^2} \frac{\partial \tilde{s}_k}{\partial \theta_i} \frac{\partial \tilde{s}_k}{\partial \theta_j}$$

$$E \left[ -\frac{\partial^2 \ln f}{\partial N_t \partial \theta_i} \right] = L \sum_{k=1}^K \frac{1}{\tilde{s}_k^2} \frac{\partial \tilde{s}_k}{\partial \theta_i} \quad (20)$$

and the derivatives of  $s_k$  and  $p_k$  with respect to  $N_t$  and the Brown and peak parameters are detailed in [22]. After replacing these derivatives in (19), the inverse of the  $\mathbf{F}_{\text{CRB}}$  can be computed. The BAGP model parameter CRBs are defined as the diagonal elements of the resulting inverse FIM. Note that

<sup>3</sup>Note that this algorithm is available in MATLAB by the function “fminsearch.”

<sup>4</sup>A simplex of dimension  $m$  is an  $m$ -dimensional polytope defined as the convex hull of its  $m + 1$  vertices. For example, a simplex of dimension 2 is a triangle [28].

the Brown CRBs used afterward are obtained by considering the vector parameters  $\theta = (\theta_1, \theta_2, \theta_3)^T$  and a  $(4 \times 4)$  FIM. Similarly, the BGP CRBs are obtained by considering  $\theta = (\theta_1, \dots, \theta_6)^T$  and a  $(7 \times 7)$  FIM.

## VI. SIMULATION RESULTS FOR SYNTHETIC WAVEFORMS

### A. Estimation Performance

This section introduces the criteria used to evaluate the quality of the estimators resulting from the different models (Brown model, BGP, and BAGP). The quality of the estimation for synthetic waveforms can be measured by comparing the estimated and true parameters by using the root-mean-square error (RMSE)

$$\text{RMSE}(\theta_i) = \sqrt{\frac{1}{n} \sum_{\ell=1}^n [\theta_i - \hat{\theta}_i(\ell)]^2}, \quad i = 1, \dots, 7 \quad (21)$$

where  $\theta_i$  is the true parameter,  $\hat{\theta}_i(\ell)$  is the estimated parameter for the  $\ell$ th waveform, and  $n$  is the number of synthetic waveforms. In the case of a real waveform, since the true value  $\theta$  is not available, the reconstruction error (RE) can be used to evaluate the quality of an estimation method

$$\text{RE} = \sqrt{\frac{1}{K} \sum_{k=1}^K (y_k - \hat{y}_k)^2} = \frac{\|\mathbf{y} - \hat{\mathbf{y}}\|}{\sqrt{K}} \quad (22)$$

where  $\hat{y}_k$  denotes the estimated waveform obtained by replacing the unknown parameters by their estimates in  $\tilde{s}_k$  defined in (3). The average RE (ARE) given by

$$\text{ARE} = \sqrt{\frac{1}{nK} \sum_{i=1}^n \|\mathbf{y}_i - \hat{\mathbf{y}}_i\|^2} \quad (23)$$

can also be used when considering  $n$  synthetic waveforms,  $\mathbf{y}_i = (y_{i1}, \dots, y_{iK})^T$  for  $i = 1, \dots, n$ .

### B. Parameter Estimation

The first set of simulations shows that the proposed BAGP model can handle Brown waveforms. For this, we have generated synthetic signals according to (1) with a sampling time  $T_s = 3.125$  ns and parameters  $P_u = 130$ ,  $\tau = 31T_s \approx 96.9$  ns, and SWH which is varying. All results have been averaged using 300 Monte Carlo runs (with different noise realizations) for each value of SWH varying in the interval  $[0, 12]$  m. Fig. 5(a), (c), and (e) shows that similar RMSEs are obtained for the different models (Brown, BGP, or BAGP) when using the NM algorithm for parameter estimation. However, when using the NR algorithm, Fig. 5(b), (d), and (f) shows that there are slightly different RMSEs from one model to another [note that the scales are different in Fig. 5(a), (c), and (e) and Fig. 5(b), (d), and (f)]. This result can be explained since the NM algorithm provides the exact MLE, while the NR algorithm only approximates the MLE via a descent method. Note that the smallest RMSEs shown in Fig. 5(b), (d), and (f) correspond to the Brown model where few parameters are

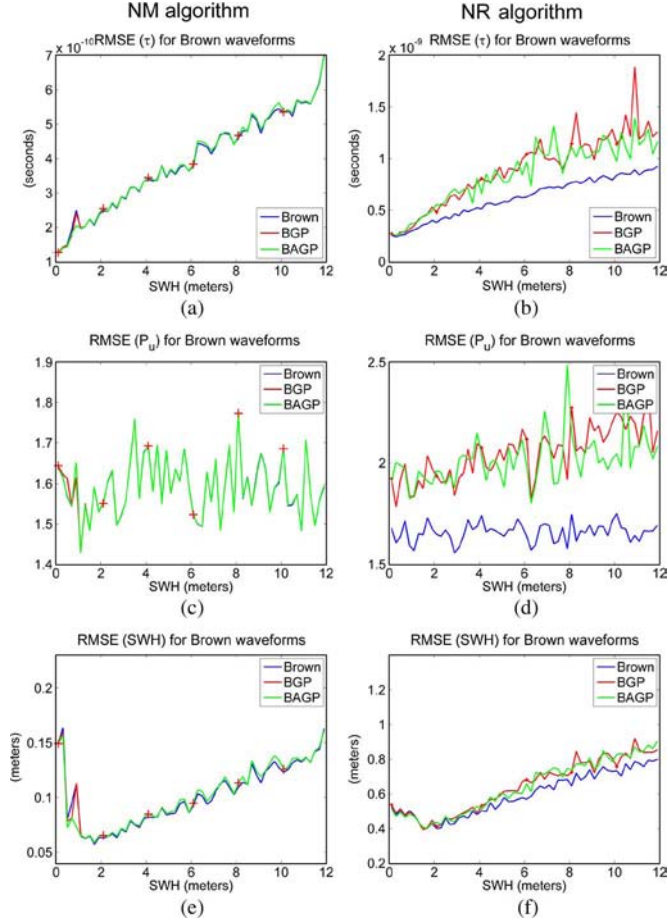


Fig. 5. Parameter RMSEs for Brown waveforms with (left) NM and (right) NR algorithms when using (blue) Brown, (red) BGP, and (green) BAGP models.

estimated. However, the estimates obtained using the other two models (BGP and BAGP) are satisfactory even if these models are not needed for Brown waveforms. Note finally that the NM method always provides better results than the NR method at the price of a higher computational time.

The second set of simulations has been obtained with synthetic waveforms similar to signals belonging to Class 13 of Fig. 2. More precisely, we have simulated Brown waveforms corrupted by a symmetric peak located in the trailing edge with the parameters  $P_u = 130$ ,  $\tau = 31T_s$  and  $A = 200$ ,  $T = 75T_s$ ,  $\sigma = 3T_s$ ,  $\gamma = 0$  (as displayed in Fig. 6(a) which shows a typical waveform of Class 13 with SWH = 2 m). Fig. 6 shows the RMSEs obtained by using the NM algorithm with the Brown and BGP models (for clarity, the RMSEs of the BAGP have not been presented here since they are very similar to those obtained with the BGP). The Brown model provides larger RMSEs since it does not take into account the peak corrupting the altimetric signal. Conversely, the BGP model shows good performance (note again that the BAGP provides very similar performance for this example). It is interesting to note that the RMSEs for the BGP model are close to the corresponding CRBs when applying the NM algorithm (see Section VI-C). Fig. 7 shows results obtained with the NR method (note that the scales are different in Figs. 6 and 7) confirming the superiority of the BGP model with respect to the Brown model for

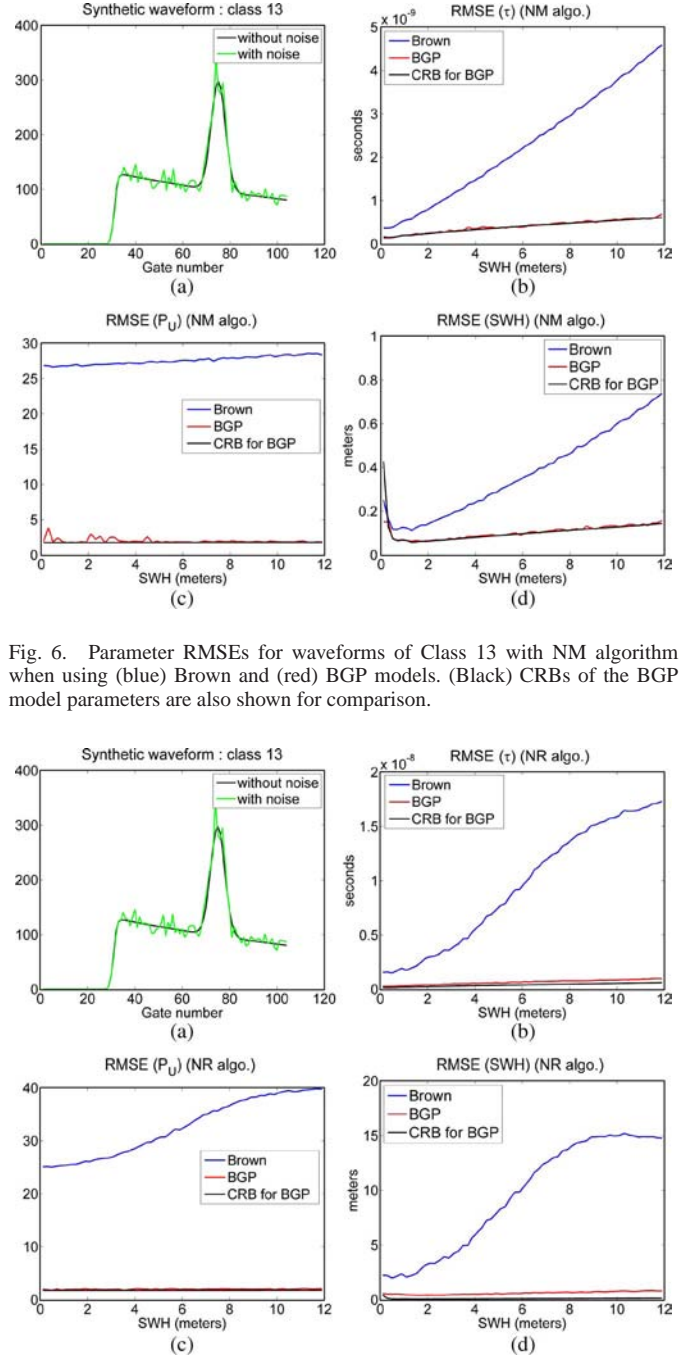


Fig. 6. Parameter RMSEs for waveforms of Class 13 with NM algorithm when using (blue) Brown and (red) BGP models. (Black) CRBs of the BGP model parameters are also shown for comparison.

Fig. 7. Parameter RMSEs for waveforms of Class 13 with NR algorithm when using (blue) Brown and (red) BGP models. (Black) CRBs of the BGP model parameters are also shown for comparison.

peaky altimetric signals. Simulations conducted for different values of  $T$  show that the estimation performance is not very sensitive to the peak location as shown in Table II for the NR algorithm. Finally, it is of increasing interest to consider the BGP and BAGP models when the peak amplitude exceeds 30% of the amplitude of the Brown model. Indeed, the traditional Brown model provides very poor performance for these values of the peak amplitude (the reader is invited to consult [22] for additional simulation results). Note that the Brown model still provides satisfactory results for small values of the peak amplitude.



TABLE II  
RMSES VERSUS PEAK LOCATION  $T$  (NR ALGORITHM)

$\frac{T}{T_s}$	65	75	85	95	105
$\text{RMSE}(\tau) (\times 10^{-10})$	8.10	7.63	7.27	7.26	7.12
$\text{RMSE}(P_u)$	2.06	2.02	1.94	1.94	1.71
$\text{RMSE}(\text{SWH})$	0.71	0.68	0.67	0.68	0.66

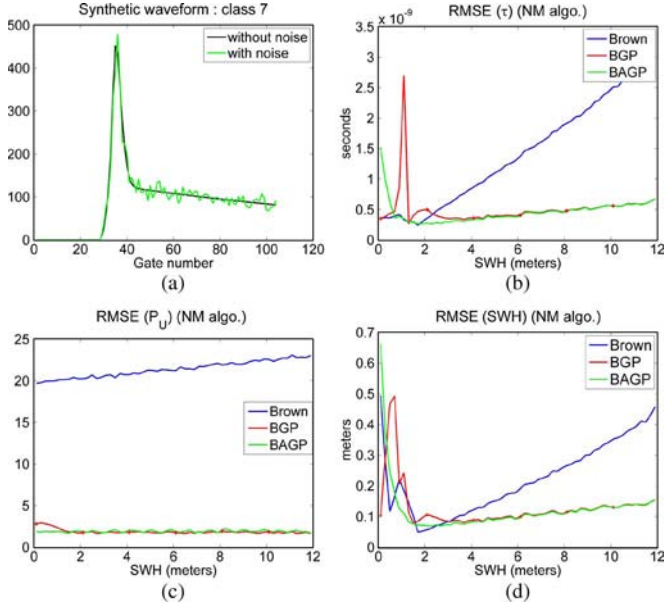


Fig. 8. Parameter RMSEs for waveforms of Class 7 with NM algorithm when using (blue) Brown, (red) BGP, and (green) BAGP models.

The third set of simulations has been conducted using synthetic waveforms with a peak located at the end of the leading edge ( $T$  is located at the maximum of the Brown model) as shown in Fig. 8(a) where  $\text{SWH} = 2$  m. The Brown and peak parameters are  $P_u = 130$ ,  $\tau = 31T_s$  and  $A = 200$ ,  $\sigma = 3T_s$ ,  $\gamma = 1/T_s$ . Fig. 8 shows the RMSEs obtained with the NM algorithm for the Brown, BGP, and BAGP models. The BGP model cannot always handle the asymmetric nature of the peak, resulting in poor estimation performance for  $\text{SWH} < 4$  m when applying the NM algorithm and for all SWHs when applying the NR algorithm (see Fig. 9). For small values of SWH, the Brown model is able to capture the leading edge [see Fig. 1(a)], leading to relatively small RMSEs for parameters  $\tau$  and SWH. However, the amplitude of the echo cannot be estimated accurately as shown in Fig. 8(c). For larger values of SWH, the performance of the Brown model decreases significantly. The BAGP model is able to model accurately the altimetric waveforms in all scenarios except for very small values of SWH. The application of the NR method confirms the superiority of the BAGP model for this class of waveforms as shown in Fig. 9 (note that the scales are different in Figs. 8 and 9). Table III shows the AREs obtained for synthetic signals from Classes 7 and 13 with the different algorithms investigated in Section IV. Note that the waveforms from Classes 7 and 13 have been generated by varying SWH and keeping the other parameters unchanged with respect to the previous experiment. It can be noticed that the proposed BAGP is very robust to different shapes of altimetric waveforms and provides very satisfactory AREs for all models. Table IV shows the corresponding exe-

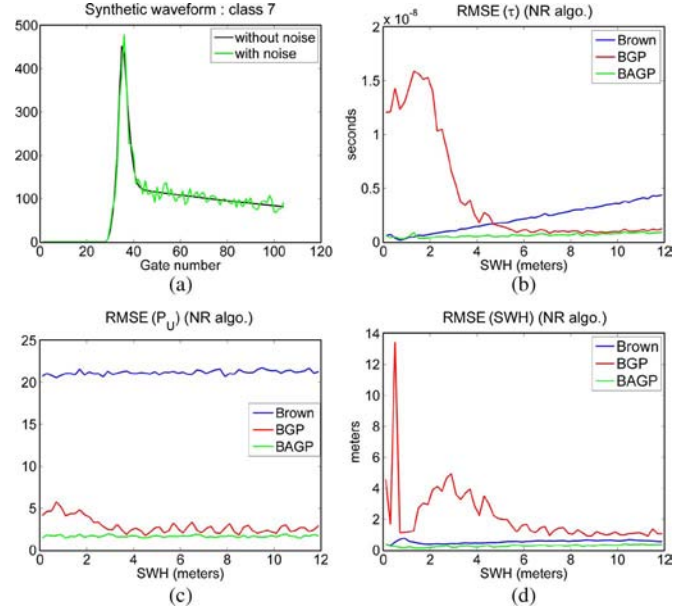


Fig. 9. Parameter RMSEs for waveforms of Class 7 with NR algorithm when using (blue) Brown, (red) BGP, and (green) BAGP models.

TABLE III  
AVERAGED RECONSTRUCTION ERRORS (SYNTHETIC DATA)

		Classes of synthetic waveforms		
		C1	C13	C7
NM	Brown	<b>8.99</b>	43.46	55.29
	BGP	<b>8.99</b>	11.10	15.12
	BAGP	<b>8.99</b>	<b>10.97</b>	<b>11.80</b>
NR	Brown	8.91	42.89	54.73
	BGP	8.75	<b>10.82</b>	20.37
	BAGP	<b>8.53</b>	<b>10.82</b>	<b>15.56</b>

TABLE IV  
AVERAGED EXECUTION TIMES IN SECONDS (SYNTHETIC DATA)

		Classes of synthetic waveforms		
		C1	C13	C7
NM	Brown	0.27	<b>0.40</b>	<b>0.28</b>
	BGP	<b>0.21</b>	0.88	0.90
	BAGP	0.24	0.98	2.73
NR	Brown	<b>0.014</b>	<b>0.018</b>	<b>0.006</b>
	BGP	0.020	0.024	0.022
	BAGP	0.244	0.375	0.257

cution times of MATLAB implementations with a 2.93-GHz i7 CPU for one altimetric waveform. These results indicate that the computational time of the BAGP estimation algorithm is reasonable even if it exceeds the one obtained with the other algorithms. From these results, we conclude that the BGP has good properties for signals corrupted by a symmetric peak located on the trailing edge of the Brown's echo (Class 13 of Fig. 2). However, it is not appropriate for waveforms of Class 7. The introduction of an asymmetric peak characterized by the asymmetry coefficient  $\gamma$  allows the BAGP to better approximate signals from Class 7. Note finally that the effects of the peak

TABLE V  
SIMULATION SCENARIO

	$P_u$	$\tau$ (s)	SWH (m)
Experiment 1 (Figs. 10.a and 10.b)	130	$31 T_s$	$\in [0, 12]$
Experiment 2 (Figs. 10.c and 10.d)	$\in [20, 170]$	$31 T_s$	5
Experiment 3 (Figs. 10.e and 10.f)	130	$\in [28 T_s, 34 T_s]$	5

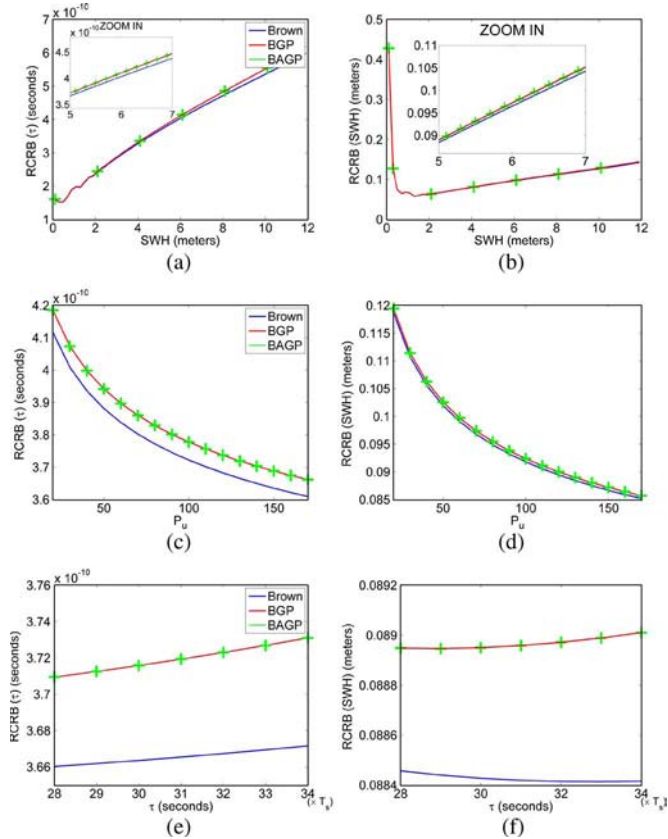


Fig. 10. RCRBs for the Brown, BGP, and BAGP models with parameter vectors  $\theta_{\text{Brown}} = (P_u, \tau, \text{SWH})^T = (130, 31T_s, 5)^T$ ,  $\theta_{\text{BGP}} = (P_u, \tau, \text{SWH}, A, T, \sigma)^T = (130, 31T_s, 5, 200, 75T_s, 3T_s)^T$ , and  $\theta_{\text{BAGP}} = (P_u, \tau, \text{SWH}, A, T, \sigma, \gamma)^T = (130, 31T_s, 5, 200, 75T_s, 3T_s, 0)^T$ . The left and right columns are associated with parameters  $\tau$  and SWH, respectively. The top, middle, and bottom figures have been obtained by varying SWH,  $P_u$ , and  $\tau$ , respectively.

is more pronounced for waveforms of Class 7 since it directly affects the leading edge of the altimetric echo.

### C. Cramér-Rao Bounds

This section studies the CRBs for the Brown, BGP, and BAGP models. We consider waveforms characterized by the peak parameters  $A = 200, T = 75T_s, \sigma = 3T_s$ , a number of looks  $L = 90$ , and different values for the parameters  $P_u, \tau$ , and SWH as shown in Table V (see [22] for the case of CRBs evaluated with other parameters). Fig. 10(a) and (b) shows the BAGP, BGP, and Brown CRBs as a function of SWH varying from 0 to 12 m. Note that varying SWH leads to a variation of the slope of the leading edge. For too small values of SWH, the slope of the leading edge is very abrupt and thus contains few

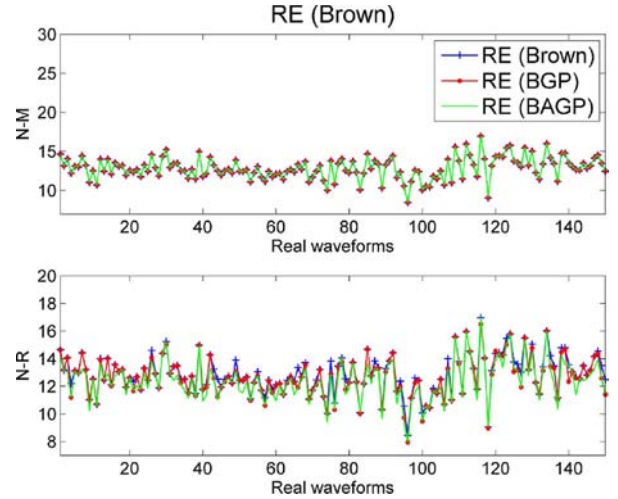


Fig. 11. REs for 150 waveforms from Class 1 with (top) NM and (bottom) NR methods.

samples, resulting in poor estimation. This corresponds to the range  $\text{SWH} \in [0, 2]$  m in Fig. 10(b). For larger values of SWH, the CRB of SWH is an increasing function of this parameter (as shown in Fig. 10(b) for  $\text{SWH} > 2$  m) since the absolute error is directly related to the value of the parameter. Fig. 10(c) and (d) shows the BAGP, BGP, and Brown CRBs as a function of  $P_u$ . Increasing  $P_u$  implies a larger impact of the Brown echo with respect to the Gaussian peak. Thus,  $\text{CRB}(\tau)$  and  $\text{CRB}(\text{SWH})$  are decreasing functions of  $P_u$ . Fig. 10(e) and (f) shows the slight influence of  $\tau$  on the CRBs of  $\tau$  and SWH. Note that the square roots of the CRBs (RCRBs) have been displayed in order to compare them with the corresponding RMSEs. Note finally that the CRBs of BGP and BAGP model parameters are larger than those of the Brown model because BGP and BAGP involve additional unknown parameters (see [22] for more results about the CRBs).

## VII. REAL JASON-2 WAVEFORMS

This section evaluates the performance of the proposed model for real JASON-2 waveforms. The classifier developed within the PISTACH project [16] was used to isolate waveforms from Classes 1 (Brown), 13 (peak on the trailing edge), and 7 (peak at the end of the leading edge). We have first considered Jason-2 waveforms. The REs obtained with these waveforms are shown in Figs. 11–13 for the different models. These results confirm that the BAGP model provides better REs than the other models. Table VI shows the averaged execution times of the different estimation algorithms for real Jason-2 waveforms. This table shows that the NM method requires more computational time than the NR method. Table VI also shows that the computational time is directly related to the number of parameters to be estimated (as expected). Fig. 1 shows typical estimated waveforms for signals of Classes 7 and 13 which allow the estimation quality to be appreciated. The BGP and BAGP provide very similar results for the signal of Class 13 since the associated peak is symmetric. However, the signal from Class 7 is better approximated by the BAGP (see,

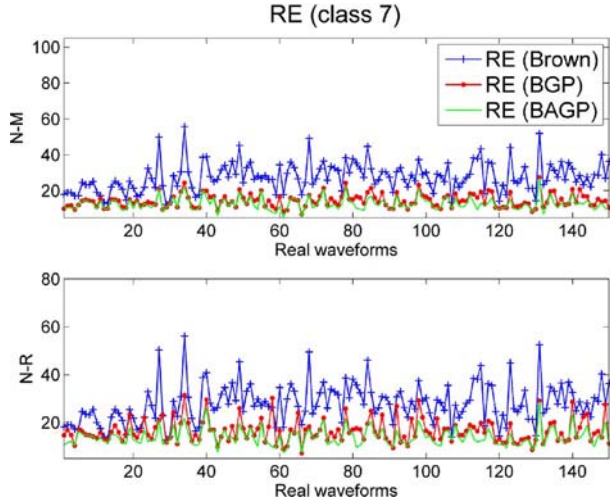


Fig. 12. REs for 150 waveforms from Class 7 with (top) NM and (bottom) NR methods.

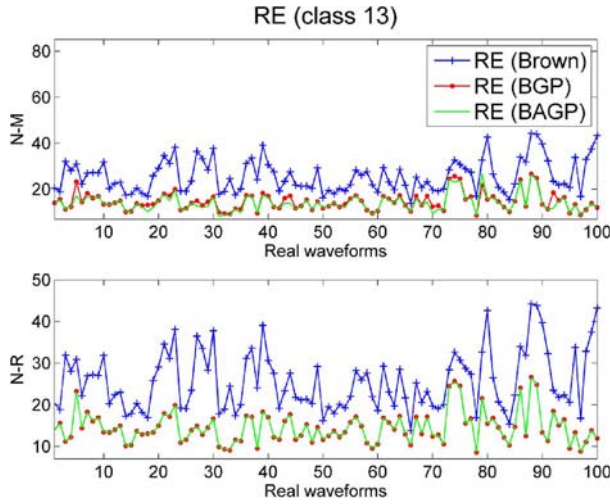





Fig. 13. REs for 100 waveforms from Class 13 with (top) NM and (bottom) NR methods.

TABLE VI  
AVERAGED EXECUTION TIMES FOR THE ESTIMATION ALGORITHMS  
IN SECONDS (REAL JASON-2 WAVEFORMS)

		Classes of real waveforms		
		 C1	 C13	 C7
NM	Brown	0.313	<b>0.206</b>	<b>0.289</b>
	BGP	<b>0.289</b>	0.541	0.668
	BAGP	0.335	1.733	1.375
NR	Brown	<b>0.013</b>	<b>0.015</b>	<b>0.009</b>
	BGP	0.018	0.022	0.024
	BAGP	0.252	0.277	0.149

in particular, the zoom on the leading edge) which allows the asymmetric peak to be estimated more accurately.

In a second step, we have considered a set of Jason-2 data obtained around Ibiza island. The Jason-2 data were extracted from the pass 187 of cycle 8 and are represented in Fig. 14 (top left). This data set shows an elliptical behavior (from latitude gate 65 to 110) which is due to the movement of the peak in the trailing edge (Class 13). Note also the presence of Class 7

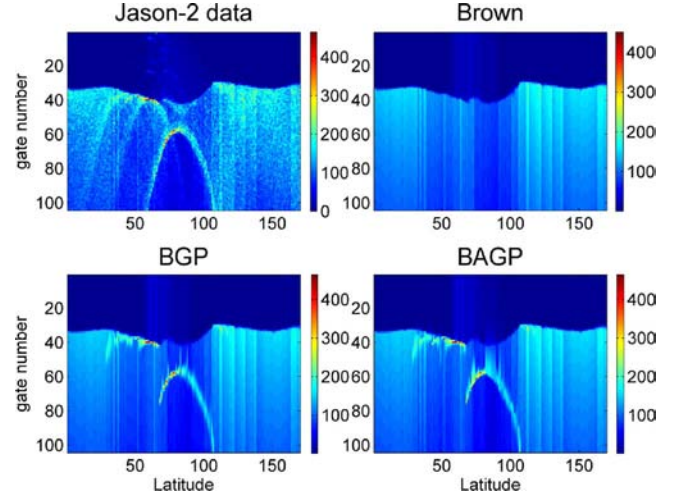


Fig. 14. Jason-2 waveforms estimated by using (top right) Brown, (bottom left) BGP, and (bottom right) BAGP models.

waveforms (from latitude gate 40 to 65) which present a high power at the end of the leading edge. The altimetric parameters of these waveforms have been estimated by using the Brown, BGP, and BAGP models. Fig. 14 shows the reconstructed waveforms for each model by using the corresponding estimated parameters. This figure shows that we get a better fit by using the BGP and BAGP models than the Brown model (see [22] for more simulation results).

## VIII. CONCLUSION

This paper studied a new model for altimetric waveforms referred to as the “BAGP” model. The parameters of this model were estimated by using the ML method. The determination of the MLE was investigated by two methods based on NR recursion and an NM algorithm, respectively. Estimations obtained with the NM method were better in terms of MSE than those obtained with the NR algorithm. However, the price to pay with the NM algorithm is a higher computational cost. Results obtained in this study showed that the proposed model can be used to retrack efficiently standard oceanic Brown echoes as well as coastal echoes corrupted by a symmetric or asymmetric Gaussian peak. This paper also derived CRBs for the parameters of the BAGP model. These bounds were used as references to which MSEs were compared. The mses of the model parameter estimates obtained using the ML principle were shown to be very close to the corresponding CRBs, illustrating the asymptotic MLE efficiency. The bounds were also used to evaluate the loss of performance for estimating the Brown parameters in the presence of a Gaussian peak. This loss of performance is mainly due to more parameters to be estimated when the model contains a symmetric or asymmetric Gaussian peak. Extending the results obtained in this paper to the four-parameter Brown model (including the mispointing as a fourth parameter) is an interesting issue. The proposed BAGP model could also be of interest for retracking echoes affected by  $\sigma$ -blooms or rain cells. These points are currently under investigation.

## REFERENCES

- [1] G. Brown, "The average impulse response of a rough surface and its applications," *IEEE Trans. Antennas Propag.*, vol. AP-25, no. 1, pp. 67–74, Jan. 1977.
- [2] A. Rius, E. Cardellach, and M. Martin-Neira, "Altimetric analysis of the sea-surface GPS-reflected signals," *IEEE Trans. Geosci. Remote Sens.*, vol. 48, no. 4, pp. 2119–2127, Apr. 2010.
- [3] G. Alberti, L. Festa, C. Papa, and G. Vingione, "A waveform model for near-nadir radar altimetry applied to the Cassini mission to Titan," *IEEE Trans. Geosci. Remote Sens.*, vol. 47, no. 7, pp. 2252–2261, Jul. 2009.
- [4] P. Naenna and J. Johnson, "A Monte Carlo study of altimeter pulse returns and the electromagnetic bias," *IEEE Trans. Geosci. Remote Sens.*, vol. 48, no. 8, pp. 3218–3224, Aug. 2010.
- [5] J.-P. Dumont, "Estimation optimale des paramètres altimétriques des signaux radar Poséidon," Ph.D. dissertation, Institut National Polytechnique de Toulouse, Toulouse, France, 1985.
- [6] E. Rodriguez, "Altimetry for non-Gaussian oceans: Height biases and estimation of parameters," *J. Geophys. Res.*, vol. 93, no. C11, pp. 14 107–14 120, 1988.
- [7] S. Maus, C. M. Green, and J. D. Fairhead, "Improved ocean-geoid resolution from retracked ERS-1 satellite altimeter waveforms," *Geophys. J. Int.*, vol. 134, no. 1, pp. 243–253, Jul. 1998.
- [8] D. T. Sandwell and W. H. F. Smith, "Retracking ERS-1 altimeter waveforms for optimal gravity field recovery," *J. Geophys. Res.*, vol. 163, pp. 79–89, 2005.
- [9] J. Severini, C. Mailhes, J.-Y. Tourneret, and P. Thibaut, "Bayesian estimation of altimeter echo parameters," in *Proc. IEEE IGARSS*, Boston, MA, 2008, vol. 3, pp. III-238–III-241.
- [10] J. Tournadre, J. Lambin-Artru, and N. Steunou, "Cloud and rain effects on AltiKa/SARAL Ka-band radar altimeter—Part I: Modeling and mean annual data availability," *IEEE Trans. Geosci. Remote Sens.*, vol. 47, no. 6, pp. 1806–1817, Jun. 2009.
- [11] J. Tournadre, J. Lambin-Artru, and N. Steunou, "Cloud and rain effects on ALTIKA/SARAL Ka-band radar altimeter—Part II: Definition of a rain/cloud flag," *IEEE Trans. Geosci. Remote Sens.*, vol. 47, no. 6, pp. 1818–1826, Jun. 2009.
- [12] C. Desportes, E. Obligis, and L. Eymard, "On the wet tropospheric correction for altimetry in coastal regions," *IEEE Trans. Geosci. Remote Sens.*, vol. 45, no. 7, pp. 2139–2149, Jul. 2007.
- [13] C. Desportes, E. Obligis, and L. Eymard, "One-dimensional variational retrieval of the wet tropospheric correction for altimetry in coastal regions," *IEEE Trans. Geosci. Remote Sens.*, vol. 48, no. 3, pp. 1001–1008, Mar. 2010.
- [14] F. Mercier, G. Dibarboure, C. Dufau, L. Carrere, P. Thibaut, E. Obligis, S. Labroue, M. Ablain, P. Sicard, G. Garcia, T. Moreau, L. Commien, G. Valladeau, N. Picot, J. Lambin, E. Bronner, A. Lombard, A. Cazenave, J. Bouffard, M.-C. Gennero, F. Seyler, P. Kosuth, and N. Bercher, "The PISTACH project for coastal altimetry: Status, products and early results," in *Proc. OST-ST Meeting*, Seattle, WA, 1998.
- [15] S. Vignudelli, A. G. Kostianoy, P. Cipollini, and J. Benveniste, Eds., *Coastal Altimetry*. Berlin, Germany: Springer-Verlag, 2011.
- [16] P. Thibaut and J. C. Poisson, "Waveforms processing in PISTACH project," in *Proc. 2nd Coastal Altimetry Workshop*, Pisa, Italy, 2008.
- [17] J. Gómez-Enri, S. Vignudelli, G. D. Quartly, C. P. Gommenginger, P. Cipollini, P. G. Challenor, and J. Benveniste, "Modeling ENVISAT RA-2 waveforms in the coastal zone: Case study of calm water contamination," *IEEE Geosci. Remote Sens. Lett.*, vol. 7, no. 3, pp. 474–478, Jul. 2010.
- [18] J.-Y. Tourneret, C. Mailhes, J. Severini, and P. Thibaut, "Parameter estimation for peaky altimetric waveforms," in *Proc. Oceans From Space*, Venice, Italy, Apr. 26–30, 2010.
- [19] L. Amarouche, P. Thibaut, O. Z. Zanife, J.-P. Dumont, P. Vincent, and N. Steunou, "Improving the Jason-1 ground retracking to better account for attitude effects," *Marine Geodesy*, vol. 27, no. 1/2, pp. 171–197, 2004.
- [20] J. A. Nelder and R. Mead, "A simplex method for function minimization," *Comput. J.*, vol. 7, no. 4, pp. 308–313, 1965.
- [21] M. Kendall and A. Stuart, *The Advanced Theory of Statistics. Vols. II*. London, U.K.: Charles Griffin & Comp. Limited, 1961.
- [22] A. Halimi, C. Mailhes, J.-Y. Tourneret, P. Thibaut, and F. Boy, "Parameter estimation for peaky altimetric waveforms," Univ. Toulouse-CLS-CNES, Toulouse, France, Tech. Rep. [Online]. Available: <http://halimi.perso.enseiht.fr/>
- [23] G. D. Quartly, M. A. Srokosz, and A. C. McMillan, "Analyzing altimeter artifacts: Statistical properties of ocean waveforms," *J. Atmos. Ocean. Technol.*, vol. 18, no. 12, pp. 2074–2091, Dec. 2001.
- [24] D. P. Bertsekas, *Nonlinear Programming*. Belmont, MA: Athena Scientific, 1995.
- [25] C. Mailhes, J.-Y. Tourneret, J. Severini, and P. Thibaut, "Cramér–Rao bounds for radar altimeter waveforms," in *Proc. EUSIPCO*, Lausanne, Switzerland, Aug. 28, 2008.
- [26] P. J. Green, "Iteratively reweighted least squares for maximum likelihood estimation, and some robust and resistant alternatives," *J. R. Stat. Soc. Ser. B, Methodol.*, vol. 46, no. 2, pp. 149–192, 1984.
- [27] J. C. Lagarias, J. A. Reeds, M. H. Wright, and P. E. Wright, "Convergence properties of the Nelder–Mead simplex method in low dimensions," *SIAM J. Optim.*, vol. 9, no. 1, pp. 112–147, 1998.
- [28] W. Rudin, *Principles of Mathematical Analysis*, 3rd ed. New York: McGraw-Hill, 1976.

**Abderrahim Halimi** (S'11) received the Eng. degree in electronics from the Nationale Polytechnic School of Algiers, Algeria, in 2009 and the M.Sc degree in signal processing from the Institut National Polytechnic de Toulouse, Toulouse, France, in 2010. He is currently working toward the Ph.D. degree in the Signal and Communication Group at the Institut de Recherche en Informatique de Toulouse, University of Toulouse.

His research interests are centered around hyperspectral imaging and altimetry.

**Corinne Mailhes** (M'87) received the Ph.D. degree in signal processing from the University of Toulouse, Toulouse, France, in 1990.

She is currently a Professor with the University of Toulouse, and a member of the Institut de Recherche en Informatique de Toulouse Laboratory, and a Director of the Telecommunications for Space and Aeronautics Laboratory. Her research interests include statistical signal processing, with particular interests in spectral analysis, data compression, and biomedical signal processing.

**Jean-Yves Tourneret** (SM'08) received the Ph.D. degree from the University of Toulouse, Toulouse, France, in 1992.

He is currently a Professor with the University of Toulouse and a member of the Institut de Recherche en Informatique de Toulouse. His research activities are centered around statistical signal processing with a particular interest to Bayesian algorithms and Markov chain Monte Carlo methods.

Dr. Tourneret has been a member of different technical committees, including the Signal Processing Theory and Methods committee of the IEEE Signal Processing Society (in 2001–2007 and 2010–present).

**Pierre Thibaut** received the PhD degree in electronic and signal processing from the University of Toulouse, Toulouse, France, in 1994.

In 1996, he joined the Oceanography Division of the Collecte Localisation Satellites (CLS), Toulouse, and has been involved in many studies and projects aiming at defining, developing, and improving the scientific processing of altimeter missions such as Poseidon-1, Jason-1/2, Envisat/RA-2, and Cryosat. Since 2010, he has been the Head of the Instruments and Physical Measurements Department in CLS, which is focused on altimetry and radiometry activities. He is a Jason-1 and Saral/AltiKa Co-Investigator and Jason-2 Principal Investigator.

**Francois Boy** received the Engineering degree in physics from the Ecole Centrale Marseille, Marseille, France, in 2005 and the Master degree in electronics from University of Toulouse, Toulouse, France, in 2006.

He is currently working at the Centre National d'Etudes Spatiales, Toulouse, in the altimetry and radar department. His research activities are centered around processing methods for SAR/Doppler altimetry systems (CRYOSAT and Sentinel-3 missions).